Surface effects in atomistic mechanical simulations of Al nanocrystals

Javier Munilla
Centro de Investigaciones Energéticas Medioambientales y Tecnológicas (CIEMAT), E-28040 Madrid, Spain

Mario Castro*
Grupo Interdisciplinar de Sistemas Complejos (GISC) and Grupo de Dinámica No Lineal (DNL), Escuela Técnica Superior de Ingeniería (ICAI), Universidad Pontificia Comillas de Madrid, E-28015 Madrid, Spain

Alberto Carnicero
Grupo de Dinámica No Lineal (DNL), Escuela Técnica Superior de Ingeniería (ICAI), Universidad Pontificia Comillas de Madrid, E-28015 Madrid, Spain

(Received 17 February 2009; revised manuscript received 17 June 2009; published 10 July 2009)

Detailed knowledge of the mechanical properties of nanocrystals is crucial for understanding the behavior of micromachining devices. Determining experimentally the elastic and plastic properties of nanocrystals can be very challenging. In this work, we present molecular-dynamics simulations of mechanical properties of Al nanocrystals, both using Lennard-Jones and embedded-atom method potentials. We show that this kind of tests borrowed from mechanical engineering provide helpful insight on the mechanical behavior of nanocrystals. We also provide evidence suggesting that the small scale effects, mainly due to the small surface-to-volume ratio of nanocrystals, are crucial. The main results of our work are the failure of the thermodynamical relations connecting the applied stress and the material strain (additionally, we introduce a simple mathematical framework to account for this effect), the nonequilibrium behavior at the onset of the plastic deformation related to the appearance of long tails (power law) in the distribution of dissipated heat and, finally, the existence of conditions under which the system can experience reversible load-unload cycles in the plastic state.

DOI: 10.1103/PhysRevB.80.024109 PACS number(s): 02.70.Ns, 62.20.−x

I. INTRODUCTION

Nanowires and other nanoscale materials have attracted considerable interest as active components of electronic and electromechanical devices (see Ref. 1 and references therein). The advent of nanotechnology and the maturity of certain fields as surface science or electronic microscopy have catalyzed recently many efforts focused on the critical behavior at the onset of plasticity, fracture, the dependence on scale of mechanical properties, hardening, and others.

Traditionally, most of the computational work in the field has been devoted to the connection between continuum mechanics and the atomistic point of view of matter, mainly due to the potential technological applications of nanosized materials. This is exemplified, for instance, in numerous studies of the mechanical properties of nanocrystalline materials such as metals,[2] silicon,[3] carbon nanotubes,[4] and more recently on graphene.[5] Besides, and from a theoretical and more fundamental viewpoint, the role of microscopic avalanches and the so-called plastic flow are crucial in order to understand the physical origin of plasticity, yield, and fracture.[6] It is precisely at the nanoscale where molecular dynamics has been proven fruitful to gain some insight on the influence of microscopic collective motion on macroscopic behavior.

In this scenario, molecular-dynamics allows to study the effect of collective atom motion on mechanical properties.[7] For instance, it has been recently shown that nanocrystalline fcc metals constitute a perfect testbed to stress the validity of some qualitative explanations of the apparent differences between nanocrystals and macrosolids.[8] Thus, in this work we will use also nanocrystalline fcc Al, partly due to this recent interest on fcc metals and partly because it can be simulated both accurately and consistently with experiments (as we will show below) using simple pair potentials.

In this paper, we adopt a mixed strategy to study mechanical properties of nanosized materials. By means of molecular-dynamics simulations, we perform (computer) mechanical engineering tests (common to macroscopic solids) as tensile, shear, or contact tests. This method allow us to determine the qualitative effect of surface on relevant mechanical properties. Moreover, as we can control the external actions on every single atom, we do not need to do further assumption about the connection between microscopic potential energies and macroscopic elastic constants.[9] In summary, we want to emphasize the differences between nanosingle crystals and solids made of nanosized grains due to the relevant role of the material surfaces. It is expected that the mechanical properties of single-crystal materials of hundreds to thousands of nanometers must be more relevant as miniaturization allows to build many components of micromachining at those scales.

The report of our results is organized as follows. In Sec. II, we review some concepts from continuum mechanics (such as stress-strain graphs, elastic constants, contact laws, etc.). We provide some details of our molecular-dynamics simulations in Sec. III. We emphasize the consistency of our choice of potential energies and other parameters in Sec. III B. In Sec. IV, we present our main results and we conclude in Sec. V with the highlights of our work and some outlook to future research.

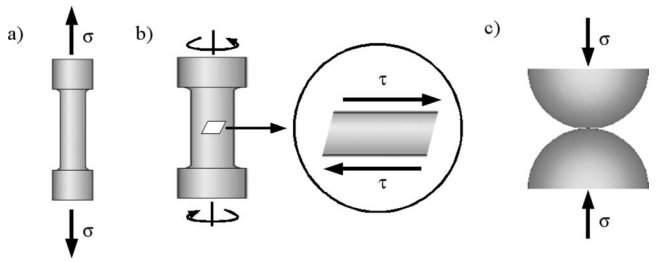

FIG. 1. Sketch of the mechanical tests performed in this work. (a) Tensile test: two uniaxial stresses σ are applied in opposite directions. (b) Torsion test: two opposite torques are applied. Internally, a material volume is subject to two antiparallel stresses, τ are applied to the material (zoomed region inside the circle). The latter situation is what we are reproducing in this work. (c) Contact test: two bodies are put in contact through a loading stress σ. In (a) and (b), the strain rate is constant, whereas in (c), the applied stress is constant.

II. MECHANICAL PROPERTIES OF MATERIALS

In this section, we summarize some concepts of continuum mechanics and introduce some notation that will follow hereafter. For an introduction to the field, see, for instance, Refs. 10 and 11.

Elasticity. Briefly, we want to distinguish between two kind of properties: elastic and contact-related properties. The elastic behavior of materials is usually characterized by three parameters (see Fig. 1): the Young's modulus E, the shear stress modulus or modulus of rigidity G, and the Poisson's ratio μ (although, in general, the first two are tensors).

These parameters help to quantify the response of a material under tensile (E) and shear (G) tests (Fig. 1). In the case of isotropic materials, they are related by

$$G = \frac{E}{2(1+\mu)}. \tag{1}$$

Besides, Poisson's ratio μ relates the strain suffered by a material in the transverse direction ε_{trans}, when it is deformed externally a magnitude ε_{axial} in the axial direction,

$$\mu = \left| \frac{\varepsilon_{trans}}{\varepsilon_{axial}} \right|. \tag{2}$$

Thermodynamics constrains the values of μ to be in the range $-1 \leq \mu \leq 0.5$, being $\mu = 1/3$ a typical value of metallic solids.[10]

Although nanoscopic fcc metals are not rigorously isotropic,[12] we will constraint our mechanical tests to preferred crystalline directions so we will not determine all the elements of E and G tensors but those in predefined orientations [so we expect that Eq. (1) can be approximately valid[13]].

Contact. Contact mechanics is usually defined as the study of the tensions and deformations suffered by two solid bodies when they are put together in contact.[14] This problem has important applications, for instance, in nanotribology, the study of granular media, or wear.[15]

Hertz's theory was the first, and to date the most used (see, for instance, an application in nanoindentation in Ref. 16 and references therein) attempt to describe the contact between solids in the elastic regime.[10] Specifically, Hertz's law states that the radius of curvature of the deformed interface a is related to the applied compressive force (load) F and material and geometrical parameters through the simple relation (for spheres, see Fig. 2 for additional notation),

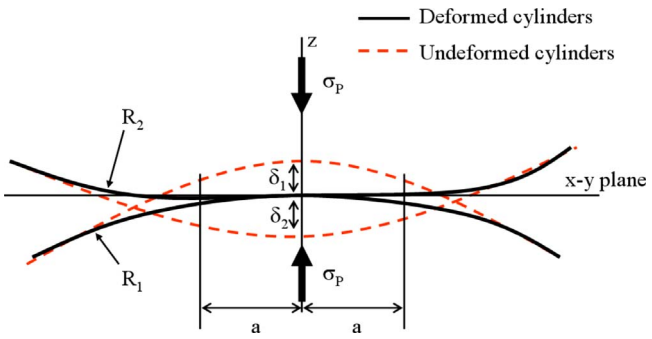

FIG. 2. (Color online) Notation used in the contact theory. In our case, we are considering two equal semispheres ($R_1 = R_2$) are put in contact through an external loading σ_P. The contact radius a and the deviation from the undeformed state $\delta_1 = \delta_2$ can be extracted numerically from this test.

$$a = \left(\frac{3FR}{4E^*} \right)^{1/3}, \tag{3}$$

with

$$\frac{1}{E^*} = \frac{1-\mu_1^2}{E_1} + \frac{1-\mu_2^2}{E_2}, \tag{4}$$

and

$$\frac{1}{R} = \frac{1}{R_1} + \frac{1}{R_2}, \tag{5}$$

where R_1 and R_2 are the radii of curvature of the solids at the contact point.

The derivation of Hertz's law is based on some assumptions besides linear elasticity, namely, the surfaces of contact must be continuum, materials are isotropic and homogeneous, there is no relative sliding between surfaces and, finally, strains are small in comparison with the mean radii of curvature of the solids. These assumptions can be strong and, in general, not valid for atomistic simulations.

Adhesion. As we have emphasized above, an important peculiarity of nanosized materials is the relevance of the events taking place at the surface. The atoms near the solid surface possess higher energy than those in the bulk due to the lack of atoms in their neighborhood. This excess energy is called the surface tension (also known as the energy of adhesion per unit area). When two different solids are close to each other, an *adhesion* force appears that tries to put the surfaces of both solids in contact. Surface tension γ can be computed as the net difference between the surface tensions before ($\gamma_1 + \gamma_2$) and after (γ_{12}) contact,

$$\gamma = \gamma_1 + \gamma_2 - 2\gamma_{12}. \tag{6}$$

In order to account for these surface phenomena, Johnson, Kendall and Roberts (JKR) (Ref. 17) proposed a theory of adhesive contact. Accordingly to the JKR theory, the relation between the applied load and the radius of curvature of the contact is given by (for equal radii $R_1=R_2=R$)

$$a^3=\frac{3R}{4E^*}[F+3\pi\gamma R+\sqrt{6\pi R\gamma F+(3\pi R\gamma)^2}]. \tag{7}$$

Note that the Hertz's law is recovered in the limit of no adhesion $\gamma\to 0$. It is customary to quantify the relevance of adhesion through an adimensional quantity called Tabor's number μ_T defined as[18]

$$\mu_T=\left[\frac{R\gamma^2}{(E^*)^2d^3}\right]^{1/3}, \tag{8}$$

where d is the average distance from an atom to its nearest neighbors. Tabor's number ranges from $\mu_T=0.000\,5$ for Hertzian contact to $\mu_T\geq 5$ for a purely adhesive contact.

III. ATOMISTIC SIMULATIONS

A. Simulation parameters and setup

In this paper, we simulate fcc Al, partly motivated by its increasing interest as a testbed system to study the dynamics of dislocations.[8] Besides, as we show in this section, it can describe accurately some structural properties of real Al.

The choice of the molecular-dynamics potentials is somehow controversial, specially for Al.[19] In principle, multiparticle potentials as embedded-atom methods (EAM) (Ref. 20) may contain more physical aspects of the microscopical interactions among atoms but—as emphasized in Ref. 19—it is unclear which of these calculations is most reliable, making an evaluation of the EAM models difficult. Thus, another aim of our work is to determine its reliability in this particular context. Other authors[21] use other pair potentials (for instance, Morse's potential) in the modeling of Al. Morse's potentials has three independent parameter [in contrast with Lennard-Jones (LJ) that has only two]. In order to be more exhaustive, in this work, we simulate both Lennard-Jones and EAM potentials. The differences between them are quantitative but, qualitatively, we obtain the same results. For LJ, we will use the following parameters:[22] $\sigma=2.62$ Å and $\varepsilon=4824$ K. Further details of both techniques can be found in Ref. 7 and references therein.

One important ingredient of molecular-dynamics simulations is the choice of the boundary conditions. Here, we consider that surfaces are free—periodic boundary conditions may inhibit the relaxation of defects at the surface (as moving dislocations or diffusional point defects).

One of the most relevant observables of our work is the stress tensor. Macroscopically, the stress is a tensor which takes into account the forces exerted per unit area on a differential volume. Microscopically, one can estimate the components of the tensor from the so-called virial stress,[23,24]

TABLE I. Structural properties of Al. Column d stands for the FCC lattice spacing and d_{nn} for the distance of an atom to its nearest neighbors.

	d (Å)	d_{nn} (Å)
Crystalline Al (experimental)	4.04	2.856
Bulk atom (MD) (Lennard-Jones)	4.04	2.857
Surface atom (MD) (Lennard-Jones)	4.10	2.897
Bulk atom (MD) (EAM)	4.04	2.856
Surface atom (MD) (EAM)	4.10	2.893

$$\sigma_{\alpha\beta}=\frac{1}{\Omega}\sum_i\left(m_iv_i^\alpha v_i^\beta+\sum_{j>i}r_{ij}^\alpha F_{ij}^\beta\right), \tag{9}$$

where the subindexes $\{ij\}=\{x,y,z\}$ stand for the components of the position and force vectors between particle α and particle β within a volume of interaction Ω. There has been some controversy about this definition but, as shown in Refs. 24–26, this definition is not compatible with macroscopic Cauchy stress when averaged over space and time. Thus, another alternative expression is commonly used,

$$\sigma_{\alpha\beta}=\frac{1}{\Omega}\sum_i\sum_{j>i}r_{ij}^\alpha F_{ij}^\beta, \tag{10}$$

In order to overcome this controversy and provided that we can track the force exerted on every atom, we will calculate the stress from the microscopic forces (and areas) of the atoms being under action of the external forces.

B. Physical consistency of the simulations

Our choice for LJ potential is based, among other reasons, on its capability to reproduce well-known properties of Al, as the fcc structure or the lattice spacing. EAM potentials are fitted to provide additional benefits (as the melting point, for instance). We are interested in the mechanical response of the nanocrystal, so, we will focus on the lattice organization of the material. In Table I, we summarize the values of the lattice spacing and distance to nearest neighbors for both experiments and molecular-dynamics simulations, showing a good agreement.

Due to the relevance of the surface-to-bulk ratio, we have computed the mentioned parameters for the atoms located at the materials surface. Clearly, the lattice spacing is larger in that case due to the lack of bonds between surface atoms with respect with those at the bulk. For both potentials (LJ and EAM), the ratio between the lattice parameter for surface atoms 4.10 and bulk atoms 4.04 is about 1.4%, which is in agreement with the experimental known values for Al.[27] Note that both potentials give, approximately, the same structural values. Thus, the main differences between them are related to binding energies, so we expect that qualitatively the results are independent of the potential choice.

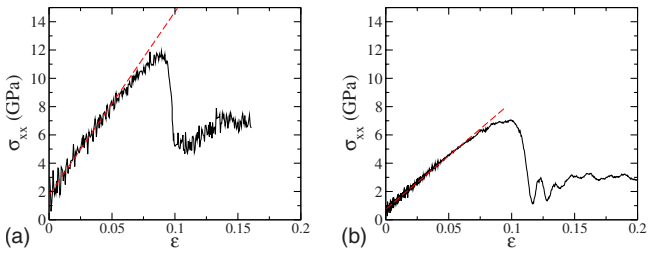

FIG. 3. (Color online) Stress-strain curve obtained from the tensile tests for a $70\times50\times50$ Å^3 crystal containing approximately 10^4 atoms. The straight dashed line is a linear fit in the elastic region of slope E. Note that this fit does not cross through the origin. This is a manifestation of the effect of the surface tension (see text). (a): simulations performed with Lennard-Jones potential $E_{\mathrm{LJ}}=149.6$ GPa. (b): simulations performed with EAM potential $E_{\mathrm{EAM}}=86.7$ GPa.

IV. RESULTS

In the preceding section, we have checked the validity of the LJ and EAM potentials to capture the structural features of Al. Now, we report on three types of mechanical tests to Al nanocrystals (as sketched in Fig. 1): tensile, shear, and contact tests. In all cases, we extract the elastic properties of the nanocrystal from the analysis of the morphological response of the system and not from questionable coarse-grained formulas connecting the microworld and the macroworld as discussed in Sec. III A and not by means of Eqs. (9) and (10). This can be done because we know at every time step the exact position, velocity, and force exerted by/over all the atoms.

A. Tensile tests

Tensile tests are performed by applying two opposite uniaxial forces to a 10^4 Al atom nanocrystal ($70\times50\times50$ Å^3, a typical size for monatomic nanoparticles[28]), which is deformed with a chosen strain rate of 3×10^8 s^{-1} (as in Ref. 8, in opposition to constant applied force simulations). All the simulations are made at $T=100$ K. The applied stress is plotted against the strain ε in the so-called stress-strain curve (Fig. 3).

1. Elasticity, homogeneous and heterogeneous plasticity

Although we are only considering here the case of a constant strain rate, we have performed constant stress simulations and, quantitatively, the same values for the elastic parameters were obtained (not shown). We can recognize three stages in Fig. 3: linear, homogeneous plastic, and bottleneck formation (with subsequent heterogeneous plastic deformation).

In the first regime, there is a linear relation between the stress and the strain. The slope of the curve is Young's modulus.[29] In our case, we find $E_{\mathrm{LJ}}=149.6\pm0.3$ GPa for LJ and $E_{\mathrm{EAM}}=86.7\pm0.2$ GPa for EAM. For macroscopic Al, it has been reported that $E=77$ GPa.[30] This value is in reasonable good agreement with EAM but considerably lower than the value for LJ. Other choices as Morse's potential provide $E_{morse}=27$ GPa, which underestimates the real value.

Another interesting feature that can be extracted by a simple inspection of Fig. 3 is that the stress-strain curve at the linear regime does not cross through the origin, namely, the applied stress for vanishing strains is not zero. As we analyze in Sec. V, this is one of the most notable surface effects (and will be mathematically justified in Sec. IV C).

After the linear stage (at the so-called yield point), the deformation is no longer elastic and is known as (homogeneous) plastic deformation. This stage is dominated by the creation of defects and the consequent relaxation of the internal stresses. The mechanism of yielding is not clearly understood at a microscopic level.[6,31] Notwithstanding, as we show in Sec. IV A 2, this stress release takes place in the form of avalanches which dissipate energy from larger scales to smaller ones (as in fluid turbulence). In principle, the creation of defects is related to the phenomenon of hysteresis, namely, the system displays memory effects. This is the classical explanation why polycrystalline materials are more ductile due to the relaxation of energy through grain boundaries.[2,8]

However, the scenario can be slightly different for nanocrystals due to the small surface-to-volume ratio. Thus, defects are released on the surface more easily than in the macroscopic case. In Fig. 4, we show a load-unload cycle, namely, the system is stretched from its undeformed state at constant strain rate. After, the systems are driven back to a situation in which the total length of the system is the original one.

Although there is some kind of hysteresis (the paths are unequal in the stretching and compressing stages and the stress at zero strain is slightly different), the system can be driven back to a state which is almost identical energetically.

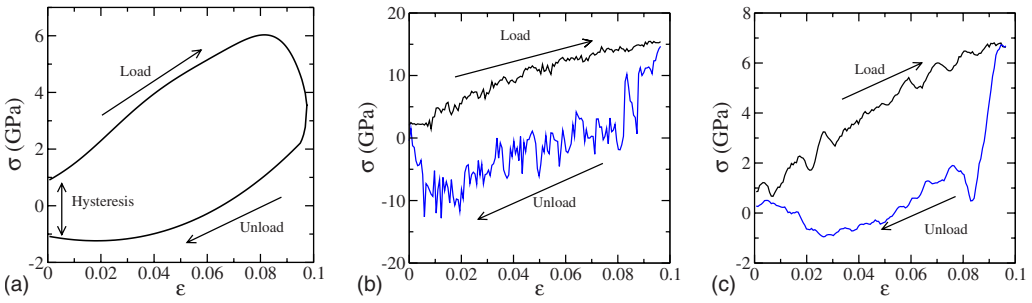

FIG. 4. (Color online) Load-unload cycle in the plastic regime. Note how, contrary to what happens in macroscopic materials (a), the plastic deformation can almost be removed reversibly (the unload curve drives the system to its initial undeformed state). There are slight differences due to some energetic differences at the surface. (b): Lennard-Jones. Bottom: EAM. Upper curves in all panels stand for loading and (c) curves for unloading.

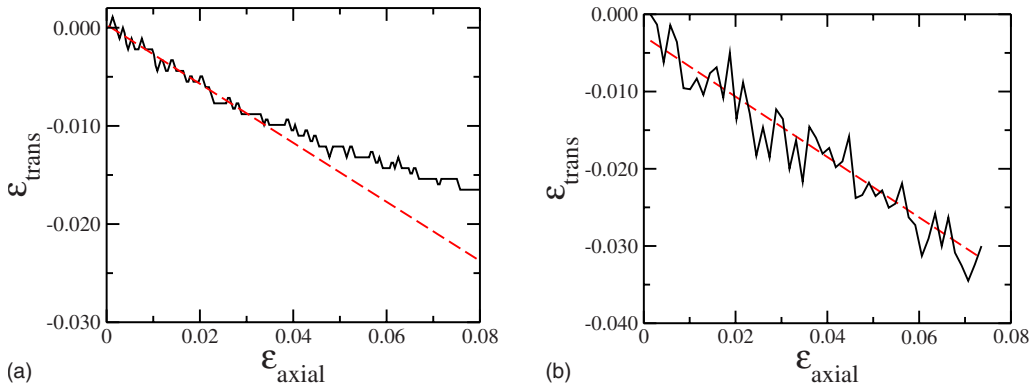

FIG. 5. (Color online) Strain rate in the transverse direction against the strain in the axial (tensile) direction in a tensile test. The absolute value of the slope of the linear fit (dashed straight line) is the value of the Poisson's ratio. (a): Lennard-Jones, $\mu=0.30$. (b): EAM, $\mu=0.31$

This happens because defect releasing at the surfaces that help the atoms to be in regular lattice positions is easier for smaller crystals. Note that the applied stress is sometimes negative (compression) in order to let the atoms accommodate to their equilibrium positions.

Finally, if the system is further deformed, due to the small size of the system and the crystalline structure of the lattice, the material may fracture or deform nonhomogeneously (for instance, through the formation of bottlenecks).

The tensile tests also allow to determine the value of Poisson's ratio μ, as given by Eq. (2). Thus, the geometrical analysis of the obtained morphologies provides the curve in Fig. 5. The straight line is a linear fit that corresponds to $\mu=0.30\pm0.01$ for LJ and $\mu=0.31\pm0.01$ for EAM, values which are close to the expected value for metals $\mu=0.33$ which is *exactly* the value for Al.

2. Energy spectrum

As the strain rate is constant, the force must change dynamically at every simulation step to accommodate to the local microscopic rearrangement of the atoms. To illustrate this fact, the fluctuations of the applied force are depicted in Fig. 6.

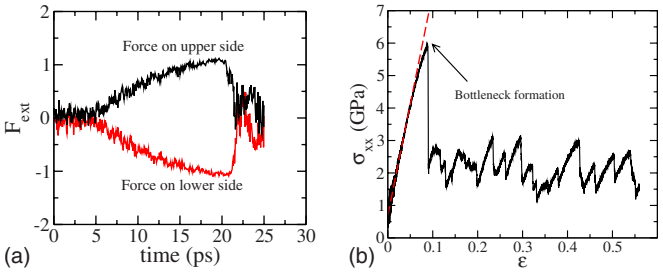

FIG. 6. (Color online) (a): time evolution of the applied forces on topmost and bottom-most layers of the material. The bottleneck formation point can be identified with the abrupt drop in the absolute value of the forces for LJ. (b): time evolution of the stress (for EAM). Plastic avalanches are related to abrupt changes in the stress. The dashed straight line shows the deviations from the linear elastic regime.

An alternative way to characterize the microscopic dynamics of the system is through the evolution of the total energy of the system. As we are performing a work to stretch the crystal, the total energy of the system is not conserved (Fig. 7). We can identify different stages of the simulation in Fig. 7 (top panel). After the yield point, the crystal is absorbing and releasing energy with the environment through its coupling with the external force. Small energy-loss events take place prior to catastrophic events as both bottleneck formation or fracture. For ductile materials, fracture is energetically less favorable than for brittle ones, and the plastic deformation is composed by a sequence of avalanches as shown in the bottom panel of Fig. 7.

Another consequence of the microscopic rearranging of the atoms is that the energy is pumped into the system in small jumps. This energy is transferred from the macroscopic modes (the macroscopic strain of the box) to the microscopic degrees of freedom. Those small magnitude strain events are precursor to the largest ones (either fracture or bottleneck formation, depending on the conditions and width of the sample). Therefore, there is a balance between inflow and

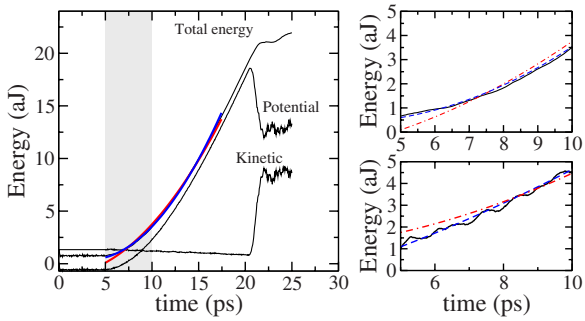

FIG. 7. (Color online) Left: time evolution of the total, potential, and kinetic energies of the material in a tensile test. The stress is applied after an equilibration stage of 5 ps. The black solid line shows the results from simulations; the dot-dashed red line is a fit to classical Hooke's law and the dashed blue line a fit to Eq. (17) for LJ potential. Right: a zoom of the region where the deviations from the classical theory are more important (gray band in left panel). In this case, both LJ (top right) and EAM (bottom right) are shown in detail.

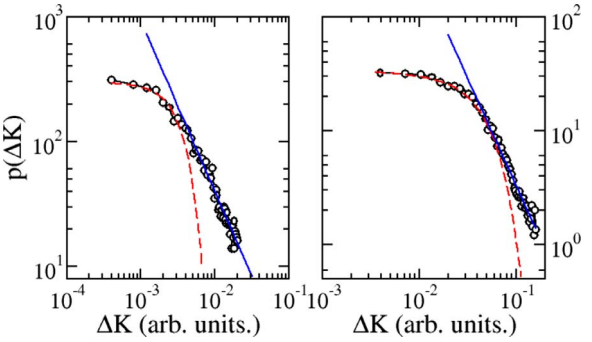

FIG. 8. (Color online) Frequency of kinetic-energy jumps (or, equivalently, heat losses). Circles stand for simulations; the dashed red line is a fit to a Gaussian. The straight solid blue line is a power-law fit of the form $(\Delta K)^{\zeta}$ showing the nonequilibrium character of plastic deformation. Left: Lennard-Jones, $\zeta_{LJ}=1.36$. Right: EAM, $\zeta_{EAM}=1.87$.

loss of energy (which one can assume, that is, lost in the form of acoustic emission). We can calculate the spectrum of acoustic emission through the distribution of kinetic-energy differences ΔK at consecutive time steps.[31] In Fig. 8, we show the deviations from a Gaussian and the power-law dependence of the acoustic spectrum after the onset of the plastic regime. The power-law dependence for high frequencies (large energy jumps) of the density resembles the Kolmogorov's energy cascade in turbulence. Actually, both phenomena are a consequence between the separation of scales that take place in the problem. In our case, we can compare the velocity of the individual atoms [which is typically on the order of $(K_BT/m)^{1/2}$] and the velocity of deformation of the crystal due to the external stress exerted on the system.

Although it is beyond the scope of the present paper, we expect that the energy cascade in Fig. 8 can play an important role on the onset of the so-called plastic flow driven by avalanches[6,31,32] which is typically a nonequilibrium process. This deviations from a Gaussian are less important for larger system sizes, in which thermodynamical fluctuations are recovered.[33] The numerical value of the exponent in the power-law part of the curve ζ could be measured in experiments or used to test analytical approaches to the problem. Characterizing whether that exponent is universal can be a numerical challenge and would need extensive simulations at different scales (and also many realizations of the same configuration, in order to improve ensemble averages). Actually, it depends on the choice of the potential: $\zeta_{LJ}=1.36$ and $\zeta_{EAM}=1.87$.

B. Torsion (shear) tests

The aim of shear tests is the computation of the modulus of rigidity G. The configuration of the shear test is shown in Fig. 1(b). In Fig. 9, we show the output of a shear test. It is noticeable that the linear regime extends hardly upon the value of the strain where fracture or bottleneck formation appears. In other words, the homogeneous plastic regime does not seem to be relevant in shear tests under the conditions considered here. As in the case of the tensile tests, we deform the nanocrystal at constant strain rate so the applied

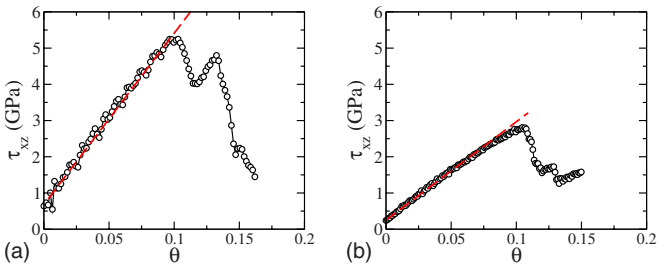

FIG. 9. (Color online) Shear stress test of a $70\times50\times50$ Å^3 crystal containing approximately 10^4 atoms. The red dashed straight line is a linear fit with slope G. (a): Lennard-Jones, $G_{LJ}=47.3$ GPa. (b): EAM, $G_{EAM}=31.6$ GPa.

force fluctuates about its mean. The value of the modulus of rigidity obtained from numerical calculations is $G_{LJ}=47.3\pm0.02$ GPa for LJ potential and $G_{EAM}=31.6\pm0.03$ GPa for EAM. For macroscopic Al, it has been reported that at 100 K, $G=29$ GPa (Ref. 30) in excellent agreement with EAM simulations and consistent with Eq. (1).

As we mentioned in Sec. II, Eq. (1) provides a consistency relation among E, G and μ. In our case, the value obtained of G_{EAM} numerically from simulations differs in less than 4%. This relation holds despite it is only strictly valid for isotropic materials because we have chosen both the tensile and shear directions not contained in the fcc slip plane (the $\langle 111\rangle$ plane).

C. Contact tests

One of the most relevant aspects of the mechanics of nanocrystals is the behavior of the materials under contact. We have simulated the contact of two solid surfaces as sketched in Fig. 1(c). Thus, two semispheres (with 5×10^3 atoms each) are compressed to each other in the direction perpendicular to the plane so sliding can be safely neglected. In all cases, we have considered the contact under constant applied stress.

The small dimensions of the system must reflect the discrete nature of the atomic composition of the material. In Fig. 10, we show the evolution of the mean separation between the centers of the two semispheres as a function of time. Note how, in all cases, there is an oscillation in the separation between both spheres. Thus parameters as the radius of curvature of the contact area a, appearing in Eqs. (3) and (7), need to be averaged over several periods. Interestingly, the frequency of oscillation is a function of the applied stress so the dynamic response is in fact a nonlinear effect (anharmonicity) of the microscopic underlying dynamics (inset in Fig. 10).

1. Numerical insight on the anharmonic behavior

The anharmonicity can be explained by means of the so-called effective potential.[34] Thus, a multiparticle stochastic dynamics can be easily described in terms of a coarse-grained effective potential as long as the dynamics is stationary. For a single particle, it is defined as

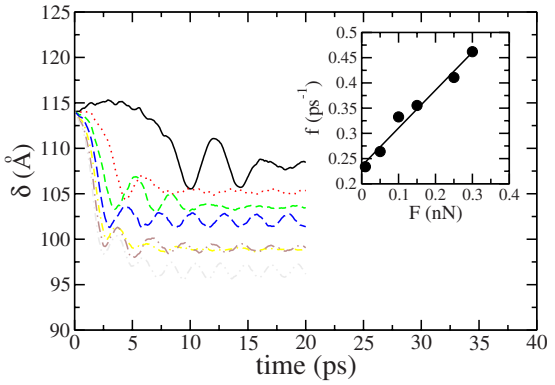

FIG. 10. (Color online) Distance between semispheres centers in a contact test. Colors stand for different values of the applied force. From top (black) to bottom (light gray): F=0.01, 0.05, 0.1, 0.15, 0.2, 0.25, and 0.3 nN, respectively. Inset: frequency of oscillation against the applied force (circles). The straight line is guide for the eyes. The anharmonicity is reflected in the nonconstant value of f.

$$V_{eff}(x) = -K_B T \log P(x), \tag{11}$$

where T is the temperature, K_B is the Boltzmann's constant, and $P(x)$ is the normalized frequency distribution of finding a particle at distance x from its equilibrium position. Note that we call V_{eff} *effective* because $P(x)$ can depend on temperature [and so it does not appear exclusively as a prefactor in Eq. (11) as in equilibrium statistical mechanics].

In Fig. 11, we show the effective potential V_{eff}, averaging over 1000 bulk particles at constant temperature and in mechanical equilibrium in a transversal direction (x). Although the particles are subject to a two-pair LJ potential, the collective coupling with its neighbors changes considerably the potential the particle actually *sees*. Thus, the constrained motion caused by the neighborhood of the particle limits the distances r the particle can explore from its equilibrium position.

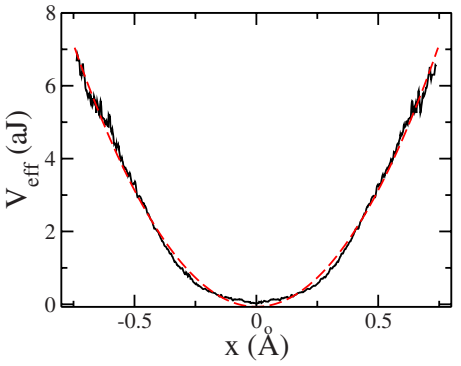

FIG. 11. (Color online) Effective potential (solid black line) V_{eff} averaged over 1000 bulk particles at constant temperature (T =100 K) and in mechanical equilibrium in the transversal direction x. The red dashed line is a fit to a parabola. Clearly, the effective potential the particles actually see is no harmonic, so a dependence of the frequency of oscillation with the applied force is expected (as in Fig. 10).

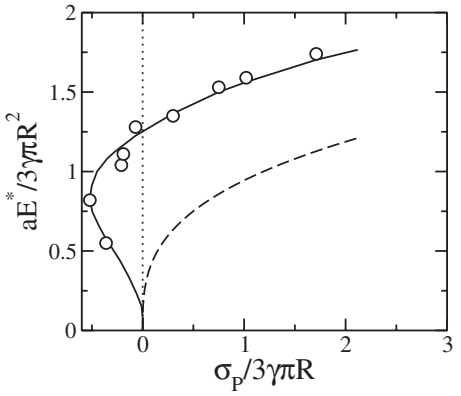

FIG. 12. Normalized radius of contact (a) against the normalized applied loading stress σ_P. The solid line is a fit to the JKR theory given by Eq. (7). The dashed line shows the prediction of Hertz's theory.

2. Surface adhesion

To quantify the importance of adhesion, we can estimate the value of the Tabor's number from the simulation data. Thus, from the definition of surface energy U_S,

$$U_S = -\gamma A_{contact} \simeq \gamma l^2, \tag{12}$$

where γ is the energy of adhesion per unit area and $A_{contact}$ is the mean area of contact between two surface atoms. From the simulations, we find that

$$\gamma_{\mathrm{LJ}} = 0.024 \ \ \mathrm{aJ/Å^2}, \tag{13}$$

and

$$\gamma_{\mathrm{EAM}} = 0.008 \ \ \mathrm{aJ/Å^2}. \tag{14}$$

Then, Tabor's number is approximately $\mu_T \simeq 0.25 \gg 0.000\,5$ for LJ and $\mu_T \simeq 0.12 \gg 0.000\,5$ for EAM, so the effects of adhesion must be important.

In Fig. 12, we show the quantitative good agreement between JKR theory and simulations (σ_P is the applied load to the spheres). Note that the surface adhesion is negligible in macroscopic Al in spite of the effect of adhesion raises with the area of contact because the contact between two macroscopic Al solids is nonconformal: two macroscopic surfaces are rough and the number of contact points depend on the applied force.[14,35] Although we have not quantified the kinetic-energy-loss distribution $f(\Delta K)$ in the contact process, it is expected that a similar energy cascade will also occur in this situation due to the so-called adhesion hysteresis.[36]

3. Mathematical approach

With the information obtained from the contact tests in the preceding section, we can sketch a mathematical theory of the deviations of the stress-strain curves from the macroscopic behavior in the limit of no strain. In other words, the fact that the stress-strain curve does not crosses through the origin. This effect comes from the importance of the surface tension in the energy balance of the system. Thus, considering an isotropic solid (for simplicity, generalizations to a tensor equation is straightforward), the external force applied

to the material in a tensile test contributes to two effects: stretching the solid and overcoming the surface tension. Thus, we can compute the elastic and surface contributions as

$$F_{ext} = F_{el} + F_{surf} = E\varepsilon L_x L_y + 2\gamma(L_x + L_y), \tag{15}$$

so

$$\sigma_{ext} = E\varepsilon + \hat{\sigma}_o \equiv E\varepsilon + 2\gamma(L_x^{-1} + L_y^{-1}), \tag{16}$$

where $L_{x,y,z}$ are the dimensions of the crystal (the tensile stresses are applied in the z direction). The first term is a consequence of Hooke's law and the second comes from the definition of surface tension (which can be equally seen as an energy per unit area or a force per unit length). Clearly, in a stress-strain plot, there is always an excess stress in the limit $\varepsilon \to 0$. Equation (16) also explains why this effect cannot be quantified for large systems. Thus, when $L_{x,y} \to \infty$, $\hat{\sigma}_0 \to 0$.

Similarly, the total energy of the crystal per unit volume is

$$e_T = \frac{dE_T}{dV} = e_0 + \frac{E\varepsilon^2}{2} + 2\gamma\varepsilon\left(\frac{1}{L_y} + \frac{1}{L_x}\right), \tag{17}$$

where e_0 is an arbitrary reference energy.

The value of the surface tension computed above (0.024 aJ/Å^2 for LJ and 0.008 aJ/Å^2 for EAM) explains the systematic deviations in the stress-strain graph. Thus, a fit to Eq. (16) in the elastic regime in Fig. 3 gives

$$\hat{\sigma}_0 = 1.76 \text{ GPa} \tag{18}$$

for LJ and

$$\hat{\sigma}_0 = 0.67 \text{ GPa}, \tag{19}$$

which is close to the value obtained from Eq. (16): $\hat{\sigma}_0 = 1.89$ GPa for LJ and $\hat{\sigma}_0 = 0.59$ GPa for EAM. Finally, in the right panels in Fig. 7, we plot a fit to Eq. (17) with and without the surface-tension term (see caption for details).

In summary, Eqs. (16) and (17) provide an experimental framework for measuring surface tensions alternative to indentation tests and a clear-cut evidence of the role of surface energy in the mechanical response of nanocrystals.

V. CONCLUSIONS

In this work, we have presented mechanical tests (borrowed from mechanical engineering) by means of molecular-dynamics simulations to characterize the elastic and homogeneous plastic regimes of Al nanocrystals. Our work has focused on the effects of the small scale and the role of the surface in the mechanical properties of the nanocrystal.

The main results of this work are (i) we have found that some thermodynamical relations in the linear regime also hold at the nanoscale as, for instance, Eq. (1), but others need to be generalized. In particular, the linear relation between the applied stress and the material strain in the elastic regime must be corrected to include surface-tension effects, as proposed in Eq. (16). This effect can also be computed through the total energy of the system [Eq. (17)]. Hence, we conclude that not only we might use tensile tests as an alternative way to measure surface tensions but also points out that the stresses needed to deform a nanocrystal must be raised in order to overcome surface-tension effects. (ii) Another consequence of the small size of the system is the importance of the relaxation from large to small degrees of freedom. Thus, the system cannot relax locally to equilibrium and the energy pumped into the system (or equivalently, the dissipated heat) possesses non-Gaussian tails typical of many small-sized systems.[37] (iii) We have shown that nanocrystals may experience reversible load-unload cycles contrary to the expected hysteresis behavior well known in macroscopic systems. Again, this reversibility is a side effect of the role of the surfaces in the problem that help to release at them the defects created in the plastic regime. (iv) Finally, the choice of the interatomic potential (either LJ or EAM) changes the previous conclusions only quantitatively (for instance, the elastic constants, or the energy of adhesion) but not qualitatively. Table II shows a comparison between potentials.

TABLE II. Comparison between Lennard-Jones and EAM potentials.

Property	Symbol (unit)	LJ	EAM
Young's modulus	E (GPa)	149.6	86.7
Modulus of rigidity	G (GPa)	47.3	31.6
Poisson's modulus	μ	0.30	0.31
Energy of adhesion	γ(aJ/Å^2)	0.024	0.008
Zero-strain stress	$\hat{\sigma}_0$ (GPa)	1.76	0.67
Spectrum exponent	ζ	1.36	1.87

Other authors have used Morse's potential for Al.[21] This kind of potential has three free parameters (in contrast with LJ which has only two), so it is more flexible. Thus, different parameters provide different results (more brittle or more ductile, for instance). In Ref. 21, the authors find that the yield stress is almost the same than in our simulations although the yield strain is considerably larger. More importantly, they also observe non-negligible zero-strain stresses in the stress-strain curves although they do not discuss this fact in the main text. This is a clear indication, at the light of our work, of surface-tension effects.

Similarly, in Ref. 32, all the stress-strain curves reported display a non-negligible zero-strain stress $\hat{\sigma}_0$, but the authors do not discuss it either.

Other authors, as Heino *et al.*,[38] use *ab initio* effective medium potentials for fcc copper. They find that both the Young's and shear moduli do not depend on the system size. This result is compatible with ours as they are estimating this values from the slope of the stress-strain curve at $\varepsilon = 0$ but, as in the preceding references, they are not considering the surface-tension effects. In other words, the slope is independent of the value of the stress at zero strain.

The role of the nanocrystal surface has indirectly been emphasized in recent molecular-dynamics simulations of ductile fracture by Sen and Buehler.[39] Although, these authors focus in the dynamics of fracture, they find that there are intrinsic length scales that depend not only on the material but also on the geometry of the experiment. Thus, the dynamics changes dramatically when the surface is confined.

Notwithstanding, our work also opens many questions that deserve extensive numerical simulations. For instance, the role of grain boundaries in nanocrystals (which can be crucial also in micrometer-length nanowires) or the diffusional creep under compressive loading need more attention. Finally, in order to make other quantitative predictions a systematic analysis of other parameters as temperature or the concentration of impurities which have straightforward applications in engineering may be done.

ACKNOWLEDGMENTS

This work has been partially supported by MEC (Spain) through Grant No. FIS2006-12253-C06-06.

*Author to whom correspondence should be addressed; marioc@upcomillas.es

[1] B. Wu, A. Heidelberg, and J. Boland, Nature Mater. **4**, 525 (2005).
[2] M. Meyers, A. Mishra, and D. Benson, Prog. Mater. Sci. **51**, 427 (2006).
[3] V. I. Ivashchenko, P. E. A. Turchi, and V. I. Shevchenko, Phys. Rev. B **75**, 085209 (2007).
[4] R. Ruoff and D. Lorents, Carbon **33**, 925 (1995).
[5] S. Stankovich, D. Dikin, G. Dommett, K. Kohlhaas, E. Zimney, E. Stach, R. Piner, S. Nguyen, and R. Ruoff, Nature (London) **442**, 282 (2006).
[6] M. Miguel, A. Vespignani, S. Zapperi, J. Weiss, and J. Grasso, Nature (London) **410**, 667 (2001).
[7] M. Buehler, *Atomistic Modeling of Materials Failure* (Springer Science & Business Media, LLC, New York, 2008).
[8] E. Bitzek, C. Brandl, P. M. Derlet, and H. Van Swygenhoven, Phys. Rev. Lett. **100**, 235501 (2008).
[9] E. Weinan and P. Ming, Arch. Mech. **183**, 241 (2006).
[10] L. Landau, E. Lifshitz, J. Sykes, W. Reid, A. Kosevich, and L. Pitaevskii, *Theory of Elasticity* (Butterworth-Heinemann, Oxford, Boston, 1995).
[11] P. Haupt, *Continuum Mechanics and Theory of Materials* (Springer, New York, 2002).
[12] Macroscopic materials are polycrystalline so isotropy is restored at large enough scales.
[13] It can be shown that in fcc crystals, several relations hold for the components of the elastic tensors that make it almost isotropical (see Ref. 20 for details).
[14] K. Johnson, *Contact Mechanics* (Cambridge University Press, New York, 1987).
[15] J. Frenken, Nat. Nanotechnol. **1**, 20 (2006).
[16] V. Navarro, O. R. de la Fuente, A. Mascaraque, and J. M. Rojo, Phys. Rev. Lett. **100**, 105504 (2008).
[17] K. Johnson, K. Kendall, and A. Roberts, Proc. R. Soc. London, Ser. A **324**, 301 (1971).
[18] J. Greenwood, Proc. R. Soc. London, Ser. A **453**, 1277 (1997).
[19] J. Zimmerman, H. Gao, and F. Abraham, Modell. Simul. Mater. Sci. Eng. **8**, 103 (2000).
[20] M. S. Daw and M. I. Baskes, Phys. Rev. B **29**, 6443 (1984).
[21] R. Komanduri, N. Chandrasekaran, and L. Raff, Int. J. Mech. Sci. **43**, 2237 (2001).
[22] J. Haile, *Molecular Dynamics Simulation* (Wiley, New York, 1997).
[23] D. Tsai, J. Chem. Phys. **70**, 1375 (1979).
[24] M. Zhou and D. McDowell, Philos. Mag. A **82**, 2547 (2002).
[25] J. Zimmerman, E. Webb III, J. Hoyt, R. Jones, P. Klein, and D. Bammann, Modell. Simul. Mater. Sci. Eng. **12**, S319 (2004).
[26] M. Buehler and H. Gao, *Modeling Dynamic Fracture Using Large-Scale Atomistic Simulations* in Dynamic Fracture Mechanics, edited by A. Shukla, (World Scientific, Singapore, 2006).
[27] C. Kittel and P. McEuen, *Introduction to Solid State Physics* (Wiley, New York, 1996).
[28] V. V. Hoang and T. Odagaki, Phys. Rev. B **77**, 125434 (2008).
[29] W. Hosford, *Mechanical Behavior of Materials* (Cambridge University Press, New York, 2005).
[30] W. Callister, *Materials Science and Engineering: An Introduction* (John Wiley & Sons, New York, 1993).
[31] F. Csikor, C. Motz, D. Weygand, M. Zaiser, and S. Zapperi, Science **318**, 251 (2007).
[32] L. Pastor-Abia, M. Caturla, E. Sanfabián, G. Chiappe, and E. Louis, Phys. Rev. B **78**, 153410 (2008).
[33] T. Hill, *Thermodynamics of Small Systems* (Dover, New York, 2002).
[34] M. Castro and G. Lythe, SIAM J. Appl. Dyn. Syst. **7**, 207 (2008).
[35] B. Persson, *Sliding Friction: Physical Principles and Applications* (Springer, New York, 2000).
[36] M. Falvo, R. Taylor II, A. Helser, V. Chi, F. Brooks, Jr., S. Washburn, and R. Superfine, Nature (London) **397**, 236 (1999).
[37] F. Ritort, Adv. Chem. Phys. **137**, 31 (2008).
[38] P. Heino, H. Häkkinen, and K. Kaski, Europhys. Lett. **41**, 273 (1998).
[39] D. Sen and M. J. Buehler, Phys. Rev. B **77**, 195439 (2008).